Synthesis of Hierarchically Porous Silica and Metal Oxide Beads Using Emulsion-Templated Polymer Scaffolds

ARTICLE *in* CHEMISTRY OF MATERIALS · OCTOBER 2004

Impact Factor: 8.35 · DOI: 10.1021/cm0492944

5 AUTHORS, INCLUDING:

Han Zhang
Peking University
398 PUBLICATIONS **6,031** CITATIONS
SEE PROFILE

Georgina Hardy
Aston University
9 PUBLICATIONS **223** CITATIONS
SEE PROFILE

Yaroslav Z Khimyak
University of East Anglia
92 PUBLICATIONS **3,889** CITATIONS
SEE PROFILE

Synthesis of Hierarchically Porous Silica and Metal Oxide Beads Using Emulsion-Templated Polymer Scaffolds

H. Zhang, G. C. Hardy, Y. Z. Khimyak, M. J. Rosseinsky, and A. I. Cooper*

Donnan and Robert Robinson Laboratories, Department of Chemistry, University of Liverpool, Crown Street, Liverpool L69 3BX, United Kingdom

Received May 3, 2004. Revised Manuscript Received August 13, 2004

Uniform, hierarchically porous inorganic beads (SiO_2, Al_2O_3, TiO_2, and ZrO_2) have been produced using emulsion-templated polymer beads as templates. The polymer scaffolds were prepared by oil-in-water-in-oil (O/W/O) sedimentation polymerization (Zhang, H.; Cooper, A. I. *Chem. Mater.* **2002**, *14*, 4017). The inorganic beads were prepared by simply immersing the polymer scaffold beads in a range of inorganic precursor solutions, followed by sol−gel condensation in air and subsequent calcination of the polymer phase. The hierarchical structures are composed of mesopores (diameters 2−5 nm), micropores (in the case of silica beads), and large emulsion-templated macropores of around 5−10 μm. All of the pores are highly interconnected. The inorganic beads exhibit high macropore volumes as characterized by mercury intrusion porosimetry. Polymer−silica composite beads with micropores and high macropore volumes were also produced. These large inorganic beads (diameters 1.0−1.5 mm) are easily handled and separated and may be useful in applications such as catalysis and separation, especially for macromolecules or viscous systems where large pores are needed to improve mass transport into the pore structure.

Introduction

Porous materials have numerous applications in the areas of catalysis, chromatography, and separation, where control over pore structure and pore size strongly influences the efficiency of the material. Materials with ordered micro- or mesopores can be prepared by templating surfactants or copolymers.[1] Ordered macroporous materials have been prepared by self-assembly of microspheres,[2] whereby an inorganic precursor is introduced into the interstices of a close-packed microsphere array and allowed to solidify before removing the microsphere template by calcination. Another method for making macroporous inorganic materials is emulsion templating: typically, a reactive metal alkoxide precursor is emulsified in the polar continuous phase of an emulsion, and macroporous materials are generated by chemical gelation of the emulsion.[3] For example, a titanium alkoxide precursor was emulsified in the droplets of an emulsion, and a titania foam was produced with a pore structure consisting of densely packed spherical shells.[4]

Materials with hierarchical porosity—that is, interconnected pores of more than one size regime—can combine the advantages of high surface areas with the increased mass transport associated with macropores. For example, MCM-41 materials with bimodal pore size distributions have been prepared using dual templating,[5] and hierarchically porous metal oxides were synthesized by a combination of micromolding, colloidal templating, and cooperative assembly of a block copolymer.[6]

Simple immersing methods have been developed where a porous polymer or other organic substrate is immersed in an inorganic precursor solution.[7−14] Or-

* To whom correspondence should be addressed. E-mail: aicooper@liv.ac.uk. Tel: 0044 151 7943548. Fax: 0044 151 7943588.

(1) (a) Kresge, C. T.; Leonowica, M. E.; Rogh, W. J.; Vartuli, J. C.; Beck, J. S. *Nature* **1992**, *359*, 710−712. (b) Lu, Y.; Fan, H.; Stump, A.; Ward, T. L.; Rieker, T.; Brinker, C. J. *Nature* **1999**, *298*, 223−226. (c) Zhao, D.; Feng, J.; Huo, Q.; Melosh, N.; Fredrickson, G. H.; Chmelka, B. F.; Stucky, G. D. *Science* **1998**, *279*, 548−552. (d) Göltner, C. G.; Berton, B.; Krämer, E.; Antonietti, M. *Chem. Commun.* **1998**, 2287−2288. (e) Yang, P.; Zhao, D.; Margolese, D. I.; Chmelka, B. F.; Stucky, G. D. *Chem. Mater.* **1999**, *11*, 2813−2826.

(2) (a) Johnson, S. A.; Ollivier, P. J.; Mallour, T. E. *Science* **1999**, *283*, 963−965. (b) Xia, Y.; Gates, B.; Yin, Y.; Lu, Y. *Adv. Mater.* **2000**, *12*, 693−713. (c) Velev, O. D.; Lenhoff, A. M.; Kaler, W. W. *Science* **2000**, *287*, 2240−2243.

(3) (a) Imhof, A.; Pine, D. J. *Nature* **1997**, *389*, 948−951. (b) Imhof, A.; Pine, D. J. *Adv. Mater.* **1998**, *10*, 697−700.

(4) Imhof, A.; Pine, D. J. *Adv. Mater.* **1999**, *11*, 311−314.

(5) (a) Davis, S. A.; Burkett, S. L.; Mendelson, N. H.; Mann, S. *Nature* **1997**, *385*, 420−423. (b) Holland, B. T.; Abrams, L.; Stein, A. *J. Am. Chem. Soc.* **1999**, *121*, 4308−4309.

(6) Yang, P.; Deng, T.; Zhao, D.; Feng, D.; Pine, D.; Chmelka, B. F.; Whitesides, G. M.; Stucky, G. D. *Science* **1998**, *282*, 2244−2246.

(7) (a) Caruso, R. A.; Antonietti, M.; Giersig, M.; Hentze, H.; Jia, J. *Chem. Mater.* **2001**, *13*, 1114−1123. (b) Schattka, J. H.; Shchukin, D. G.; Jia, J.; Antonietti, M.; Caruso, R. A. *Chem. Mater.* **2002**, *14*, 5103−5108.

(8) Retuert, J.; Quijada, R.; Arias, V. *Chem. Mater.* **1998**, *10*, 3923−3927.

(9) Maekawa, H.; Esquena, J.; Bishop, S.; Solans, C.; Chmelka, B. E. *Adv. Mater.* **2003**, *15*, 591−596.

(10) Meyer, U.; Larsson, A.; Hentze, H.; Caruso, R. A. *Adv. Mater.* **2002**, *14*, 1768−1772.

(11) Caruso, R. A.; Schattka, J. H. *Adv. Mater.* **2000**, *12*, 1921−1923.

(12) Wang, Y.; Tang, Y.; Dong, A.; Wang, X.; Ren, N.; Shan, W.; Gao, Z. *Adv. Mater.* **2002**, *14*, 994−997.

(13) Caruso, R. A.; Antonietti M. *Adv. Funct. Mater.* **2002**, *12*, 307−312.

(14) Yang, D.; Qi, L.; Ma, J. *Adv. Mater.* **2002**, *14*, 1543−1546.

10.1021/cm0492944 CCC: $27.50
Published on Web 10/08/2004

ganic−inorganic hybrid composite materials are formed by gelation of the precursors, and inorganic materials are then obtained by calcining the organic phase. For example, titania network structures were fabricated using polymer gel templating,[7] and mesoporous titania was obtained by calcination of hybrid chitosan−titania composites.[8] More recently, meso/macroporous inorganic oxide monoliths were produced from polymer foams.[9] First, a polystyrene foam monolith was synthesized by polymerization of styrene, either in the continuous or in the dispersed phase of a highly concentrated water/oil (W/O) emulsion. Second, a mixture of a self-assembling block-copolymer and a sol−gel precursor was imbibed into the macroporous foam. Porous inorganic monoliths were obtained after calcining the polymer phase.[9] Alternative synthetic polymer templates are micronsized polymer beads[10] or cellulose acetate filter membranes.[11−13] A biomimetic method for the synthesis of hierarchically porous networks composed of TiO_2 tubes was developed using eggshell-membrane templating.[14] Nanoparticles have also been used as building blocks for the preparation of porous inorganic materials; for example, synthetic copolymer gels with spongelike architectures were immersed in colloidal dispersions of Fe_3O_4 or TiO_2 to yield ceramic monoliths with macroporous structures after calcination.[15] More recently, we have used gold nanoparticles to synthesize macroporous metals using polymer scaffolds.[16]

In this paper, we have developed a templating technique that involves high internal phase emulsions (HIPEs) where the internal (or droplet) phase occupies more than 74.05% of the emulsion volume. Previously, HIPEs were used to prepare highly interconnected, open-cell polymeric materials by mixing a reactive monomer and a cross-linker in the continuous phase that was then polymerized to generate, for example, PolyHIPE materials.[17] Removal of internal phase gave rise to a porous replica of the emulsion. These highly porous, low-density materials have found applications as separation media,[18] supports for heterogeneous catalysis,[19] polymer-supported reagents,[20] and as potential tissue-engineering scaffolds.[21] The materials are usually produced as monolith blocks that conform to the dimensions of the reaction vessel,[22] and it can be relatively difficult to remove the internal phase after polymerization unless a highly volatile dispersed phase such as supercritical CO_2[23] is employed.

In extension of a method reported by Ruckenstein and Hong,[24] we have developed a technique for the preparation of monodisperse emulsion-templated polymer beads by oil-in-water-in-oil (O/W/O) sedimentation polymerization.[25] Uniform beads (bead diameters ∼2 mm) were prepared with high intrusion volumes (>8 cm^3/g) and large macropores (2−15 μm). Beaded morphologies are useful in a range of applications such as separations and catalysis. Moreover, it is much easier to remove the internal phase from these beaded materials, and the semicontinuous synthetic process can be scaled up relatively easily (i.e., by use of multiple injectors).[25]

Highly porous inorganic beads (e.g., silica, transition metal oxides) are more chemically and thermally stable than organic polymers and may thus be useful in applications such as catalysis. In a previous communication, we reported the formation of uniform, emulsion-templated silica beads with high pore volumes and hierarchical porosity.[26] In that study, a tetraethyl orthosilicate (TEOS) sol was mixed with the aqueous monomer solution, and an oil-in-water (O/W) HIPE emulsion was prepared. Hybrid emulsion-templated polymer−silica beads were obtained by O/W/O sedimentation polymerization.[26] Calcination of the polymer from the hybrid beads (520 °C) led to uniform, hierarchically porous silica beads with very high pore volumes (∼6 cm^3/g) and high surface areas (>400 m^2/g).

There are, however, a number of limitations to this technique, particularly in extending the approach to the preparation of hierarchically porous transition metal oxide beads. For example, alkoxide precursors are usually highly reactive to water and must be pretreated before formation of the O/W emulsion. Even if this precaution is taken, it is likely that the emulsion may gel before the injection process is complete. Moreover, the addition of different inorganic precursors tends to affect the stability of the HIPE emulsion, and conditions such as surfactant type and concentration must be reoptimized for each new material that is produced.

We describe here a new two-step method for the synthesis of porous emulsion-templated inorganic beads. In the first step, monodisperse porous emulsion-templated poly(acrylamide) (PAM) beads were prepared by O/W/O sedimentation polymerization.[25] The polymer beads were then used as scaffolds for the formation of inorganic−organic composite beads by immersion in a range of inorganic precursor solutions, followed by filtration and gelation of the precursors. Inorganic beads were obtained by calcining the composite. To increase the surface area or to create inorganic materials with ordered pores, a block polymer can be dissolved in the precursor solution and used as an auxiliary template. This approach represents a potentially generic method for the preparation of uniform, hierarchically porous inorganic beads from a wide range of inorganic materials such as silica, alumina, titania, and zirconia.

(15) Breulmann, M.; Davis, S. A.; Mann, S.; Hentze, H.; Antonietti, M. *Adv. Mater.* **2000**, *12*, 502−507.
(16) Zhang, H. F.; Hussain, I.; Brust, M.; Cooper, A. I. *Adv. Mater.* **2004**, *16*, 27−30.
(17) (a) Cameron, N. R.; Sherrington, D. C. *Adv. Polym. Sci.* **1996**, *126*, 163−214. (b) Ruckenstein, E. *Adv. Polym. Sci.* **1997**, *127*, 1−58.
(18) Bhumgara, Z. *Filtr. Sep.* **1995**, *32*, 245−251.
(19) (a) Ottens, M.; Leene, G.; Beenackers, A.; Cameron, N. R.; Sherrington, D. C. *Ind. Eng. Chem. Res.* **2000**, *39*, 259−266. (b) Krajnc, P.; Brown, J. F.; Cameron, N. R. *Org. Lett.* **2002**, *4*(15), 2497−2500. (c) Mercier, A.; Deleuze, H.; Maillard, B.; Mondain-Monval, O. *Adv. Synth. Catal.* **2002**, *344* (1), 33−36.
(20) Chemin, A.; Mercier, A.; Deleuze, H.; Maillard, B.; Mondain-Monval, O. *J. Chem. Soc., Perkin Trans. 1* **2001**, 366−370.
(21) (a) Busby, W.; Cameron, N. R.; Jahoda, C. A. B. *Biomacromolecules* **2001**, *2*, 154−164. (b) Busby, W.; Cameron, N. R.; Jahoda, C. A. B. *Polymer Int.* **2002**, *51*(10), 871−881.
(22) (a) Cameron, N. R.; Sherrington, D. C. *J. Mater. Chem.* **1997**, *7*(11), 2209−2212. (b) Barbetta, A.; Cameron, N. R.; Cooper, S. J. *Chem. Commun.* **2000**, 221−222. (c) Deleuze, H.; Faivre, R.; Herroguez, V. *Chem. Commun.* **2002**, 2822−2823.
(23) (a) Butler, R.; Davies, C. M.; Cooper, A. I. *Adv. Mater.* **2001**, *13*, 1459−1463. (b) Butler, R.; Hopkinson, I.; Cooper, A. I. *J. Am. Chem. Soc.* **2003**, *125*, 14473−14481.
(24) (a) Ruckenstein, E.; Hong, L. *Polymer* **1995**, *36*, 2871−2860. (b) Ruckenstein, E.; Hong, L. *Chem. Mater.* **1996**, *8*, 546−553.
(25) Zhang, H.; Cooper, A. I. *Chem. Mater.* **2002**, *14*, 4017−4020.
(26) Zhang, H. F.; Hardy, G.; Rosseinsky, M. J.; Cooper, A. I. *Adv. Mater.* **2003**, *15*, 78−81.

Table 1. Preparation Conditions and Characterization Data for Inorganic-polymer Composite Beads

samples	precursor solution[a]	mass gain (%) total (first)[b]	BET surface area (m^2/g)[c,d]	skeletal density (g/cm^3)[d]	mass loss after calcination (%)	beads shrinkage (%)[e]
C-SiO-1	TEOS sol	55.65	220	1.56	59.5	16.58
C-SiO-2[f]	TEOS sol	113.47	47	1.68	46.1	17.56
C-SiO-3	PEG-PPG-PEG + TEOS sol	182.20	2	1.43	65.5	6.34
C-AlO-1	acetone (5.20 g) + $Al(O\text{-}s\text{-}Bu)_3$ (15 mL)	110.71 (42.50)	219	1.50	66.9	11.44
C-AlO-2	PEG-PPG-PEG + 2-propanol + $Al(O\text{-}s\text{-}Bu)_3$	92.74 (33.31)	5	1.42	75.9	1.99
C-TiO-1	2-propanol (3.0 g) + $Ti(O^iPr)_4$ (10.0 mL)	98.16 (53.22)	54	1.71	58.1	10.94
C-TiO-2	PEG-PPG-PEG + $Ti(O^iPr)_4$	111.83 (33.64)	1	1.48	71.7	5.97
C-ZrO-1	$Zr(Opr)_4$ solution	175.16 (84.69)	60	2.29	44.5	13.93
C-ZrO-2	PEG-PPG-PEG + $Zr(OPr)_4$	93.74 (21.09)	5	1.69	66.7	4.48
C-SiO-4	TEOS sol	113.61	268	1.60	g	g

[a] PEG−PPG−PEG = 35.80 wt. % solution in 2-propanol for C-SiO-3, C-AlO-2, and C-TiO-2, 29 wt. % solution in 1-propanol for C-ZrO-2. Equal volumes of the block copolymer solution and the inorganic precursor solution and this resulting solution were then used to prepare samples C-SiO-3, C-AlO-2, C-TiO-2, and C-ZrO-2. [b] Mass gain was calculated based on the original PAM beads. The samples were first dried overnight at 65 °C. The values in parentheses refer to the mass gain after just one immersion in the precursor solution. [c] As characterized by N_2 sorption−desorption. [d] Samples were first dried in oven at 90 °C overnight. [e] On the basis of the average diameter of the beads before and after the sol−gel reaction and drying (calculated by measuring >100 bead diameters). [f] Formed by immersing C-SiO-1 in the precursor solution for a second time. [g] Scaled-up PAM−silica composite sample prepared for detailed N_2 sorption characterization—sample was not subsequently calcined.

Materials and Methods

Materials. For the production of porous polymer beads, the following chemicals were used: acrylamide (AM, 99+ %), *N,N′*-methylene bisacrylamide (MBAM, 99%), Triton X-405 (polyoxyethylene(40) isooctylphenyl ether, 70% w/v solution in water), poly(vinyl alcohol) (PVA, M_w = 9000−10 000 g mol^{-1}, 80% hydrolyzed), ammonium persulfate (APS, 98+%), *N,N,N,N*-tetramethylethylenediamine (TMEDA, 99.5+ %, redistilled), and mineral oil (white, light, and heavy grades).

For the preparation of inorganic/polymer composite beads, the following chemicals were used: tetraethyl orthosilicate (TEOS, 98%), aluminum tri-*sec*-butoxide ($Al(O\text{-}s\text{-}Bu)_3$, 97%), titanium isopropoxide ($Ti(OiPr)_4$, 97%), zirconium propoxide ($Zr(OPr)_4$, 70 wt % solution in propanol), and poly(ethylene glycol)-*block*-poly(propylene glycol)-*block*-poly(ethylene glycol) (PEG-*b*-PPG-*b*-PEG, 50 wt % EG content, M_w = 1900 g mol^{-1}).

A stock TEOS sol was prepared as follows: TEOS (33.75 cm^3), distilled water (10.50 cm^3), and 0.9 N HCl solution (0.15 cm^3) were mixed and sonicated in an ice−water bath to form a homogeneous solution and then stored at −20 °C for at least two weeks before use.[27]

Unless otherwise stated, all chemicals were purchased from Aldrich and used as received. Distilled water and GPR organic solvents (BDH) were used throughout.

Preparation of Porous Poly(acrylamide) (PAM) Beads. A single batch of polymer beads was prepared, as described previously,[25] and was then used as a template for the preparation of all of the subsequent inorganic materials. Briefly, the AM/MBAM solution (6.0 cm^3), Triton X-405 solution (1.3 cm^3), initiator (APS, 10 wt % aqueous solution, 0.6 cm^3), and light mineral oil (30.0 cm^3, including 0.0164 g TMEDA as redox coinitiator) were mixed with an impeller stirrer (approximately 600 rpm) to prepare a stable O/W HIPE. The oil phase was added slowly to the aqueous phase with constant stirring. Once formed, this HIPE was injected into a heated mineral oil medium (60 °C) to carry out the O/W/O sedimentation polymerization. The internal oil phase was removed by washing, and the beads were dried, as described previously.[25] Uniform emulsion-templated beads were obtained with essentially 100% conversion of monomer to polymer.

Preparation of Organic−Inorganic Composite Beads. The porous PAM beads were used as scaffolds for the formation of a range of composite materials. The general procedure was to immerse the polymer beads in an inorganic precursor solution and to soak overnight. All of the solutions (except for the TEOS sol) were placed in a fume cupboard at room temperature while soaking. The beads that were immersed in the TEOS sol were stored overnight at −20 °C because the TEOS sol was found to gel rapidly at room temperature. The soaked beads were filtered using a funnel (no filter paper was required since the beads are large) and then washed with a suitable solvent (Table 1) to remove excess precursor solution from the emulsion-templated pore structure. The beads were then placed on tissue paper and dried in air at room-temperature overnight, after which the sample was transferred into an oven at 65 °C (12 h). Any residual solvent was then removed under vacuum at the same temperature. For precursor solutions containing the block copolymer, PEG-*b*−PPG-*b*−PEG, as an auxiliary template, the precursor solutions were diluted with additional solvent by a factor of 3 just before filtration (to reduce the solution viscosity and precursor reactivity). Different solvents were used for different inorganic precursors, as described in Table 1.

Calcination of Organic Phase. It was found from previous thermogravimetric analysis (TGA) measurements[26] that mass loss for silica/cross-linked PAM composite beads continued up to around 520 °C, after which the mass remained constant. In this new study, the organic phase in the composite beads was removed by calcination in air using a Carbolite ashing furnace. The temperature was ramped from room temperature to 520 °C at 0.5 °C/min, held at this temperature for 4 h, and then cooled to room temperature at 1 °C/min. A number of samples was produced in duplicate, and the physical properties (surface area, pore volume, pore size, absolute density) were found to be reproducible to within at least ±10%.

Characterization. Low magnification optical images of the samples were recorded using a Sony DSC-S75 digital camera using the macro setting. Bead morphologies were investigated using a Hitachi S-2460N scanning electron microscope (SEM). To prepare the samples for SEM investigation, the beads were mounted on aluminum studs using carbon adhesive tape and sputter coated with a thin film of gold (~10 nm). Individual beads were sectioned with a razor to reveal the internal structure.

Nanostructural features were investigated using transmission electron microscope (JEOL-2000EX TEM) operating at 200 kV. The porous inorganic beads were ground to fine powders before analysis, and the sample grids were prepared by sonicating the powdered samples in ethanol and evaporating one drop of this suspension on a carbon coated copper grid.

Nitrogen adsorption−desorption isotherms were measured using the volumetric method with a Micromeritics ASAP 2010 analyzer at −196 °C. The samples were dried and evacuated at 110 °C before analysis. The specific surface area was calculated using the Brunauer−Emmett−Teller (BET) method using a linear plot over the range of P/P_0 0.06−0.20 (eight points collected). Pore size distributions were calculated from

(27) Brennan, J. D.; Hartman, J. S.; Ilnicki, E. I.; Rakie, M. *Chem. Mater.* **1999**, *11*, 1853−1864.

the adsorption branch of the isotherm using the Barrett, Joyner, and Halenda (BJH) method.[13,28–30] Pore volumes were determined from the amount of N_2 adsorbed at $P/P_0 = 0.90$. Macropore intrusion volumes, bulk densities, and macropore size distributions were recorded by mercury intrusion porosimetry using a Micromeritics Autopore IV 9500 porosimeter over a pressure range of 0.10 psia to 60 000 psia. Intrusion volumes were calculated by subtracting the intrusion arising from mercury interpenetration between beads (pore size >150 μm) from the total intrusion. Skeletal densities were measured using a Micromeritics Helium AccuPyc 1330 pycnometer.

The structure of the porous beads was also investigated using confocal laser scanning microscopy (CLSM, Carl Zeiss, LSM 510). To analyze the polymers, a single PAM bead was mounted on a glass slide, without adding any solvent or fluorescent dyes. A 543 nm laser was used to generate images in reflection mode. To analyze the silica beads, an isorefractive solvent mixture (DMSO/H_2O = 90:10 v/v) was prepared.[31] Nile Red was dissolved in this solvent mixture, and the silica beads were soaked in this dye solution overnight. CLSM was then conducted on a single, solvent-soaked silica bead mounted on a glass slide. A 543 nm HeNe laser was used to excite the dye that was contained in the bead pores. Two-color fluorescent images were produced by simultaneously measuring the autofluorescence of the silica by using a 458 nm argon laser.

To determine the crystal phase of the inorganic materials, X-ray diffraction (XRD) data were collected using CuKα' radiation and a position sensitive detector in capillary transmission geometry using a Stoe Stadi-P diffractometer.

Solid-state NMR spectra were recorded at 9.4 T using a Chemagnetics CMX-400 spectrometer. ^{27}Al magic-angle-spinning (MAS) NMR spectra were acquired at 104.20 MHz with pulses shorter than $\pi/10$ (0.3 μs pulse length) using zirconia rotors 4 mm in diameter spun in dry nitrogen at 8 kHz. One thousand scans were acquired with a recycle time of 0.5 s. The position of ^{27}Al resonances is quoted in ppm from external $[Al(H_2O)_6]^{3+}$.

Results and Discussion

Porous Polymer Beads. The emulsion-templated PAM scaffold beads had an average bead diameter of 2.05 mm with a standard deviation in bead diameter of 4.46% (Figure 1a). Figure 1b shows the cross-sectioned surface of a single bead, demonstrating that the HIPE structure was retained throughout the material after sedimentation polymerization and removal of internal oil phase. The porous polymer beads had an intrusion volume (macropore volume) of 6.0 cm^3/g, as measured by mercury intrusion porosimetry.[25] The pore size distribution for the beads is shown in Figure 1c. The pore structure consists mostly of macropores (average diameter = 15 μm) that correspond to the windows that connect the emulsion-templated cells.[32] The beads were also characterized using the gas sorption method and were determined to have a relatively low surface area (13.9 m^2/g). This is comparable with poly(styrene-*co*-divinylbenzene) PolyHIPE materials prepared in the absence of a solvating porogen[33] and suggests that the surface area in the materials arises from the emulsion-templated macropore structure alone: there is no appreciable meso- or microporosity in the cell walls in the dry state. This agrees with our findings for porous PAM materials produced from CO_2-in-water HIPEs.[23]

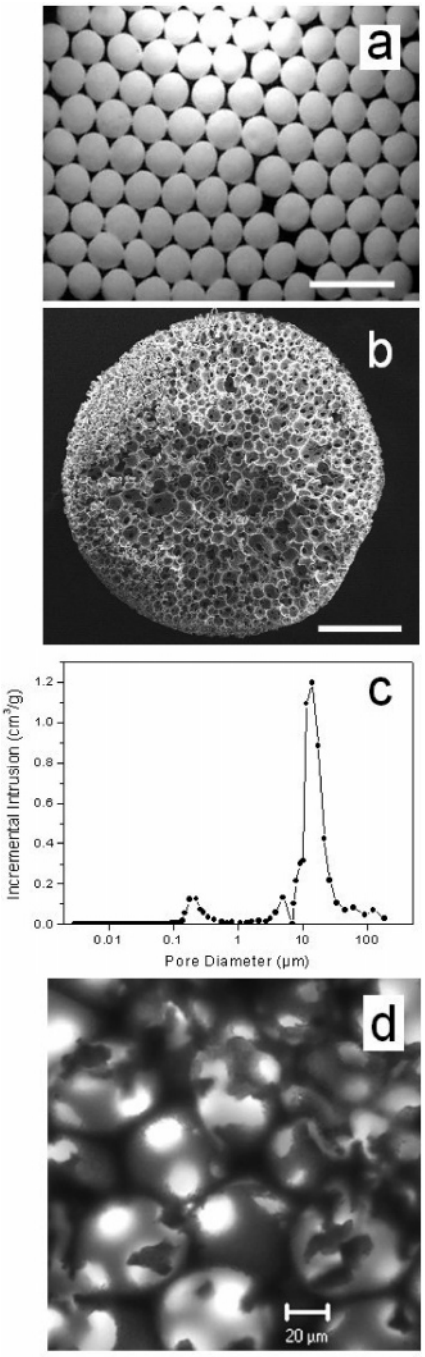

Figure 1. Original porous cross-linked polyacrylamide (PAM) beads used as scaffolds for all of the other materials present here: (a) optical image, average bead diameter = 2.05 mm, standard deviation = 4.46% (scale bar = 4.0 mm). (b) Electron micrograph of cross-sectioned bead showing the internal pore structure (scale bar = 500 μm). (c) Plot of macropore size distribution as measured using mercury intrusion porosimetry. (d) Confocal laser scanning microscopy (CLSM) image recorded using reflection mode (scale bar = 20 μm).

The highly interconnected pore structure in the beads was characterized by both SEM[25,32] and by confocal laser scanning microscopy (CLSM). CLSM has been used extensively in biology[34] and has more recently been

(28) Yao, N.; Xiong, G.; He, M.; Sheng, S.; Yang, W.; Bao, X. *Chem. Mater.* **2002**, *14*, 122–129.
(29) McIntosh, D. J.; Kydd, R. A. *Micropor. Mesopor. Mater*. **2000**, *37*, 281–289.
(30) (a) Grosso, D.; Soler-Illia, G. J.; Crepaldi, E. L.; Charleus, B.; Sanchez, C. *Adv. Funct. Mater.* **2003**, *13*, 37–42. (b) Yuan, Z.; Vantomme, A.; Leonard, A.; Su, B. *Chem. Commun.* **2003**, 1558–1559.
(31) Tallarek, U.; Rapp, E.; Sann, H.; Reichl, U.; Seidel-Morgenstern, A. *Langmuir* **2003**, *19*, 4527–4531.
(32) See Supporting Information, including optical images, SEM images, BET data, and mercury intrusion porosimetry data.
(33) Hainey, P.; Huxham, I. M.; Rowatt, B.; Sherrington, D. C. *Macromolecules* **1991**, *24*, 117–121.

explored as an analytical method in materials applications.[35] CLSM can visualize structural features in two modes: reflectance mode and/or fluorescence mode. The emulsion-templated PAM beads were analyzed using CLSM in reflection mode (Figure 1d). This showed clearly that the pores in these materials are highly interconnected and that the window size is consistent with the average pore diameter that is measured by mercury porosimetry (Figure 1c).

General Procedures for Preparation of Inorganic−Organic Composite Beads. Table 1 summarizes the preparation conditions and characterization data for the inorganic−organic composite beads formed using our new, two-step method. The cross-linked PAM beads are hydrophilic in nature and swell significantly when immersed in polar solvents, especially water. This allows the introduction of a wide range of inorganic precursors into the walls of the emulsion-templated structures. However, when the solvent-soaked PAM beads were dried directly from polar solvents such as water, it was found that the beads shrank significantly and that the shape became irregular. The HIPE-templated structure was also highly deformed during shrinkage.

For solutions that contained inorganic precursors, the hydrolysis−condensation reactions occurred simultaneously at room temperature during the drying process. Unlike the case of the untreated PAM beads, it was found that the bead shape and pore structure could be preserved in these materials, albeit with varying degrees of bead shrinkage. This is presumably because the inorganic−organic composite beads are much more rigid than the native PAM structures and thus less prone to deformation upon removal of the solvent.

When either 2-propanol or acetone was used as the solvent, bead shrinkage was found to be in the range 2−14% (Table 1). The degree of shrinkage was higher (approximately 17%) when a TEOS sol dispersed in a water−ethanol solvent mixture was employed (samples C-SiO-1 and C-SiO-2).

Silica−Polymer Composite Beads. Highly porous silica−polymer composite beads were formed by immersing the PAM beads in a TEOS sol, filtering the beads, washing out excess sol from the bead macropores, and then allowing the hydrolysis−condensation chemistry to occur in the polymer matrix over time. Sample C-SiO-1 was formed by immersing the PAM beads in the TEOS sol for 24 h before washing and subsequent sol−gel polymerization. SEM imaging for C-SiO-1[32] showed that the macroporous structure in the composite was similar to the original PAM beads. The emulsion-templated structure was retained, even though the mass had increased by 55.7%. CLSM imaging of the composite beads indicated that a thin coating of silica (thickness ~1.5 μm) was formed over the surface of the polymer scaffold and that the density of the material was higher at the surface (Figure 2a). This suggests that the composite structure was nonuniform with a greater proportion of the silica deposited on the polymer surface

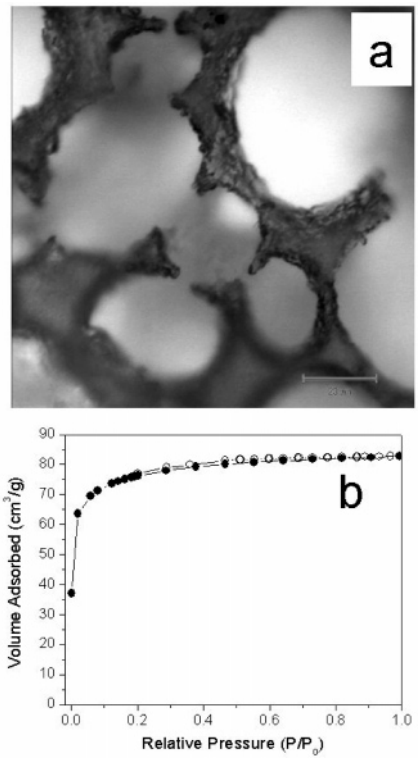

Figure 2. PAM-silica composite beads: (a) CSLM image of C-SiO-1 (scale bar = 20 μm). (b) N_2 sorption isotherms for sample C-SiO-4 (closed circles = adsorption; open circles = desorption).

but does not preclude the possibility that an interpenetrating silica-PAM network was also formed in the interior regions of the PAM scaffold.[26] To increase the silica loading in the composite, a portion of sample C-SiO-1 was treated again by immersion in a TEOS sol for a further 24 h to generate sample C-SiO-2. This second immersion led to a similar mass gain to the first immersion (total mass increase after two immersions = 113.5%), but again the emulsion-templated structure was retained, with a slight densification of the structure and an accompanying increase in the absolute density of the composite (1.68 vs 1.56 g/cm^3).

The surface area of the silica-PAM composite beads after one immersion (C-SiO-1) was found to be 220 m^2/g. This surface area was observed to decrease significantly after the second immersion in the TEOS sol to 47 m^2/g (C-Si-O-2). Gas sorption analysis showed that the isothermal curve for a similar sample (C-Si-O-4, also produced after one immersion in the TEOS sol) rose steeply at very low relative pressures indicating a type I isotherm. This indicates that a significant proportion of micropores existed in this sample (Figure 2b, micropore surface area = 221 m^2/g; total surface area = 268 m^2/g). We suggest that the second immersion leads to some in-filling of the micropores that are generated in the first immersion, thus leading to a reduction in the total surface area.

PAM−silica composite beads were also prepared by immersing the PAM scaffold material in a TEOS sol containing a block copolymer, PEG-*b*−PPG-*b*−PEG (one immersion, total immersion time = 12 h). The presence of the block copolymer had a significant effect on both the composite morphology and the BET surface area (Table 1, C-SiO-3). SEM imaging showed that the

(34) Pawley, J. B., Ed. *Handbook of Biological Confocal Microscopy*; Plenum: New York, 1995.

(35) (a) Jinnai, H.; Nakanishi, K.; Nishikawa, Y.; Yamanaka, J.; Hashimoto, T. *Langmuir* **2001**, *17*, 619−625. (b) Fergg, F.; Keil, F. J.; Quader, H. *Colloid Polym. Sci.* **2001**, *279*, 61−67.

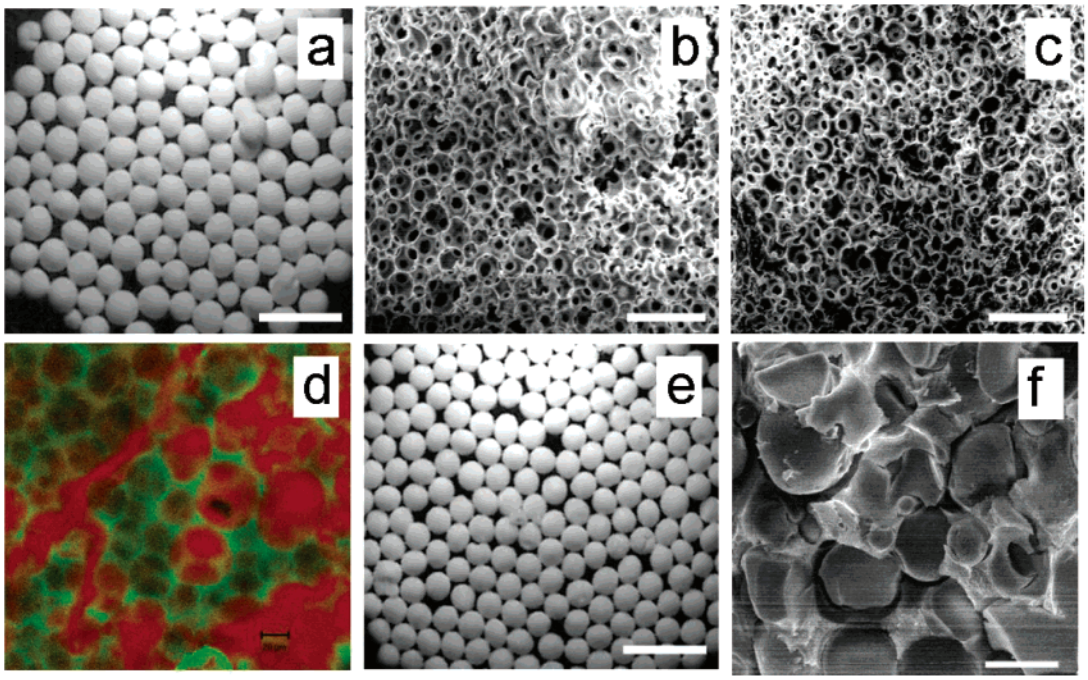

Figure 3. (a–d) Silica beads SiO-1 (no PEG-PPG-PEG template): (a) optical image (scale bar = 5 mm). (b) Electron micrograph of the cross-sectioned bead internal structure (scale bar = 100 μm). (c) Electron micrograph of the bead surface (scale bar = 100 μm). (d) Two-color CLSM image of a Nile Red solution (red) within the silica (green) matrix (scale bar = 25 μm). (e and f) Silica beads SiO-3 formed with PEG–PPG–PEG template: (e) optical image (scale bar = 5 mm). (f) Electron micrograph of the cross-sectioned bead internal structure (scale bar = 25 μm).

emulsion-templated structure was retained but that a significant proportion of the emulsion-templated cells in the composite were filled with entrapped, spherical silica miroparticles (diameter ~25 μm).[32] The number of entrapped silica particles was greatest in the center of the beads and decreased radially toward the beads surface. We believe that this is because the TEOS sol containing the block copolymer was much more viscous and that it was therefore difficult to wash the excess sol from the bead interior. As a result, excess sol was polymerized in the emulsion-templated cells to form entrapped silica microparticles, particularly within the less accessible central regions of the bead.

The surface area for sample C-SiO-3 was found to be lower than for the equivalent sample (C-SiO-1) formed without the block copolymer (2 vs 220 m^2/g). This large decrease in surface area was attributed to the presence of block copolymer in the silica material that blocked the micropore structure—indeed, calcination of sample C-SiO-3 led to a material (SiO3-3) with a much higher surface area (see next). The degree of shrinkage for sample C-SiO-3 was reduced, and the uniformity of the bead shape was also improved. This may be because additional entrapped silica fills a proportion of the emulsion-templated cells, which gives the beads a greater degree of structural rigidity.

Silica Beads after Calcination. The organic phase was removed from the PAM-silica composites by calcination at 520 °C. Figure 3a shows an optical image of a number of silica beads (SiO-1) produced by calcination of C-SiO-1. It can be seen that the beads have retained their original spherical morphology despite the large mass loss that occurs during calcination (59.5%), albeit with a shrinkage in the bead diameter of 25.4%. Figure 3b shows the internal macropore structure of a single fractured bead, while Figure 3c shows the macropore structure on the bead surface. Both SEM micrographs indicate that the original emulsion-templated pore structure has been closely replicated in the silica material—that is, the polymer has acted as a scaffold for the formation of the silica structure and this structure is retained after calcination. This is also confirmed by higher magnification SEM imaging.[32]

The calcined silica beads were also characterized using confocal laser scanning microscopy (CLSM). Figure 3d shows a CLSM image for the emulsion-templated silica beads (SiO-1). The red droplets in Figure 3d correspond to dye-containing solvent within the emulsion templated cells. Initially, the red color was distributed very evenly across the sample, which shows that the cells are highly interconnected. Not all of the cells in this image contain solvent due to partial evaporation during image capture. The silica walls can be observed as a green color that arises from the silica autofluorescence.

Figure 3e shows an optical image of the silica beads (SiO-3) obtained after calcination of C-SiO-3. This sample also retains the spherical bead morphology, although the internal structure of the beads (Figure 3f) is quite different because there are silica microparticles (diameter = ~25 μm) entrapped in a large proportion of the emulsion-templated cells (for reasons of solution viscosity, as discussed above). This is reflected in the significantly higher average bulk density for SiO-3 (0.52 vs 0.28 g/cm^3). The entrapped silica microparticles were concentrated in the bead interior and less prevalent toward the bead surface, just as in the original silica-PAM composite (C-SiO-3).

As characterized by SEM, samples SiO-1 and SiO-2 appear broadly similar. Both samples show porous

Table 2. Characterization Data for Inorganic Beads after Calcination

samples	microanalyis (%)	surface area (m^2/g)[a]	pore volume (cm^3/g)[b]	intrusion volume (cm^3/g)[c]	bulk density (g/cm^3)[d]	skeletal density (g/cm^3)[e]	macropore diameter (μm)[d]	mesopore diameter (nm)[f]	bead shrinkage (%)[g]
SiO-1	C, 0.14; H, 0.43; N, 0	260 (144)	0.16	2.82	0.28	2.29	10.5, 0.15	<3	25.37
SiO-2	C, 0.14; H, 0.18; N, 0	168 (96)	0.088	1.72	0.27	2.19	10.0, 0.15	<3	22.93
SiO-3	C, 0; H, 0.40; N, 0	644 (407)	0.25	1.03	0.52	2.27	4.0, 0.05	<3	35.12
AlO-1	C, 0.84; H, 1.99; N, 0	169 (11)	0.30	1.69	0.42	2.61	4.0, 0.08	4.0	37.81
AlO-2	C, 0.33; H, 1.80; N, 0	344 (0)	0.59	2.01	0.29	2.48	4.0, 0.08	4.0	36.32
TiO-1	C, 0.19; H, 0.42; N, 0	27 (1)	0.085	1.61	0.46	3.52	5.0, 0.08	5.0	34.33
TiO-2	C, 0; H, 0.32; N, 0	65 (0)	0.098	1.17	0.61	3.48	10.0, 0.1	4.5	39.80
ZrO-1	C, 0.37; H, 0.21; N, 0	21 (0)	0.040	0.79	0.88	4.88	10.0, 0.08	3.0	36.32
ZrO-2	C, 0.21; H, 0.20; N, 0	104 (0)	0.12	0.78	0.58	5.17	8.0, 0.04	2.5	44.78
polymer beads	C, 45.40; H, 7.68; N, 13.05	14 (5)	0.030	6.0	0.14	1.32	10.5	<2	

[a] Measured by the BET method, values in parentheses are micropore areas. [b] Pore volumes from N_2 sorption data. [c] Intrusion volumes measured by mercury porosimetry over the pore size range 7 nm to 100 μm. [d] Calculated from mercury intrusion data. [e] Measured by helium pycnometery. [f] Measured by N_2 sorption analysis. [g] On the basis of the average diameter of the beads before and after calcination.

emulsion-templated structures; however, the intrusion volumes (macropore volumes) measured by mercury porosimetry (2.82 and 1.72 cm^3/g, respectively) were considerably lower than found for the original PAM scaffolds (6.0 cm^3/g). There are two explanations for this. First, the intrusion volume is calculated per gram; as such, the intrusion volumes for samples with different skeletal densities will differ, even if the two samples have the same level of porosity. As shown in Tables 1 and 2, the silica beads have higher skeletal densities than those of the original PAM or the silica-PAM composites (PAM $\sim$1.3 g/cm^3, PAM-silica composites $\sim$1.5 g/cm^3, calcined silica $\sim$2.2 g/cm^3). The second explanation is that bead shrinkage during calcination causes a decrease in the macropore volume. The skeletal densities for the PAM beads and the emulsion-templated silica (SiO-1) were determined to be 1.32 and 2.29 g/cm^3, respectively. As such, if the decrease in macropore volume per gram were due to the increase in skeletal density alone, one would estimate the intrusion volume for SiO-1 to be $(1.32/2.29) \times 6.0 = 3.46$ cm^3/g. The fact that the intrusion volume is significantly lower than this (2.82 g/cm^3) indicates that bead shrinkage also contributes to the decrease in total macropore volume.

A type I isotherm was observed for the silica-PAM composite beads (C-SiO-1) that is consistent with a partly microporous solid with a relatively low surface area.[36] After calcining C-SiO-1, the resulting silica sample Si-O-1 showed a type II isotherm (Figure 4a), which is normally obtained with macroporous adsorbents, although the surface area obtained (Table 1) also suggests a small degree of microporosity in this sample.[36]

Sample SiO-3 exhibited a much higher surface area (644 m^2/g) of which 407 m^2/g could be attributed to micropores. The isotherm is similar to type I, but the curve rises again in the high P/P_0 range (Figure 4b). This indicates the presence of macropores. No hysteresis was observed, suggesting that well-ordered mesopores do not exist in this sample.[37] Plots of pore size distribution for the silica beads were calculated using BJH approach, again not showing mesopores.[32] The high surface area (644 m^2/g) for sample SiO-3 can potentially be explained in two ways. First, the removal of the block copolymer template from the composite by calcination may give rise to additional porosity. Second, the entrapment of silica particles in the emulsion-templated pores may lead to a material that has higher surface area than the silica that is formed on (or within the walls of) the PAM scaffold.

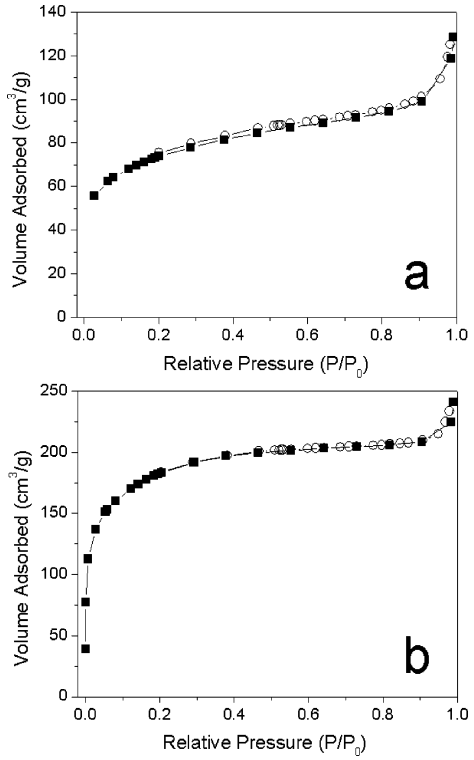

Figure 4. N_2 sorption data for calcined silica beads: (a) adsorption (closed circles) and desorption (open circles) isotherms for SiO-1. (b) Adsorption (closed circles) and desorption (open circles) isotherms for SiO-3.

Macropore size distributions, which could not be measured by N_2 sorption, were characterized for the calcined samples using mercury porosimetry. Samples SiO-1 and SiO-2 showed very similar macropore size distributions to the original PAM beads. For SiO-3, the average macropore size was smaller than for the silica beads SiO-1 and SiO-2 (4 vs 10 μm). This may arise from partial blocking of the macropores by the entrapment of silica particles in sample SiO-3. For sample SiO-3, a

(36) Sing, K. S. W.; Everett, D. H.; Haul, R. A. W.; Moscou, L.; Pierotti, R. A.; Rouquérol, J.; Siemieniewska, T. *Pure Appl. Chem.* **1985**, *57*, 603−619.

(37) (a) Sonwane, C. G.; Bhatia, S. K. *J. Phys. Chem. B* **2000**, *104*, 9099−9110. (b) Lukens, W. W.; Schmidt-Winkel, P.; Zhao, D.; Feng, J.; Stucky, G. D. *Langmuir* **1999**, *15*, 5403−5409.

bimodal macropore size distribution was observed with peaks at 4 and 0.05 μm.[32]

In our previous studies, emulsion-templated silica-PAM composite beads were prepared by a one-step sedimentation polymerization method.[26] In this case, a PAM−silica interpenetrating network was formed, and we believe that the silica was dispersed relatively homogeneously throughout the polymer matrix. A significant degree of shrinkage occurred during calcination, but the removal of the polymer phase also gave rise to additional porosity in the silica.[26] As a result, the resulting silica beads exhibited a macropore volume that was very similar to that observed in the original PAM beads (5.81 vs 5.68 cm^3/g before calcination). The surface area of these beads was high (422 m^2/g), but the micropore surface area was low (9 m^2/g). By contrast, somewhat lower surface areas and macropore volumes were observed in our new two-step method where the preformed PAM beads were immersed in a TEOS sol.

Alumina Beads. In previous studies, surfactant-assisted (cetyltrimethylammonium bromide, CTAB) synthesis was used to produce alumina with hierarchical nanopores.[38] The hierarchical structures were composed of mesopores 4 nm in diameter and macropores with diameter of about 300 nm. We show here that porous alumina beads with a trimodal pore size distribution (4.0 μm, 0.08 μm, and 4.0 nm) can be prepared using our new method. Alumina is widely used as a catalyst or catalyst support, and these materials may be very promising for catalytic reactions.

Figure 5a−c show the optical image and SEM micrographs of alumina beads AlO-2, obtained by calcining composite beads (C-AlO-2), which included a block copolymer auxiliary template. Figure 5b shows that the emulsion-templated pore structure is distributed across the whole bead. The beads surface is porous, although some of the original macropores are blocked with alumina.[32] The internal structure is very porous, and the pores are highly interconnected (Figure 5c). The internal HIPE structure was also retained for sample AlO-1 (no block copolymer auxiliary template),[32] but in this case, there were some alumina microparticles trapped in the pores, probably because the reactivity of the precursor solution was higher in the absence of the block copolymer template (i.e., there was some gelation in the sample prior to washing). The bead surface in AlO-1 was covered by a relatively dense alumina film, and only a few of the original macropores were replicated.

Alumina microparticles could be observed clearly for sample AlO-1,[32] and the number of entrapped alumina microparticles in the beads could be adjusted by varying the immersing time and the washing method. Figure 5d shows the internal structure of alumina beads that were prepared with less intensive washing (one time, normally five times), and it can be seen that most of the cells are filled with alumina microparticles.

It was found that there were three steps in the cumulative intrusion curve for sample AlO-2 (as distinct from the two-step curve observed for the original PAM scaffold material).[32] The cumulative intrusion curve for AlO-2 continues to rise at the high-pressure end, indicating the presence of smaller pores (<7 nm); this can be seen as a truncated peak in Figure 6a. The presence of mesopores is further confirmed by the type IV N_2 adsorption−desorption isotherm that shows a pronounced hysteresis (Figure 6b). The hysteresis type is not a typical one defined in the literature but seems to lie between type H_2 and H_3.[36] The BJH pore size

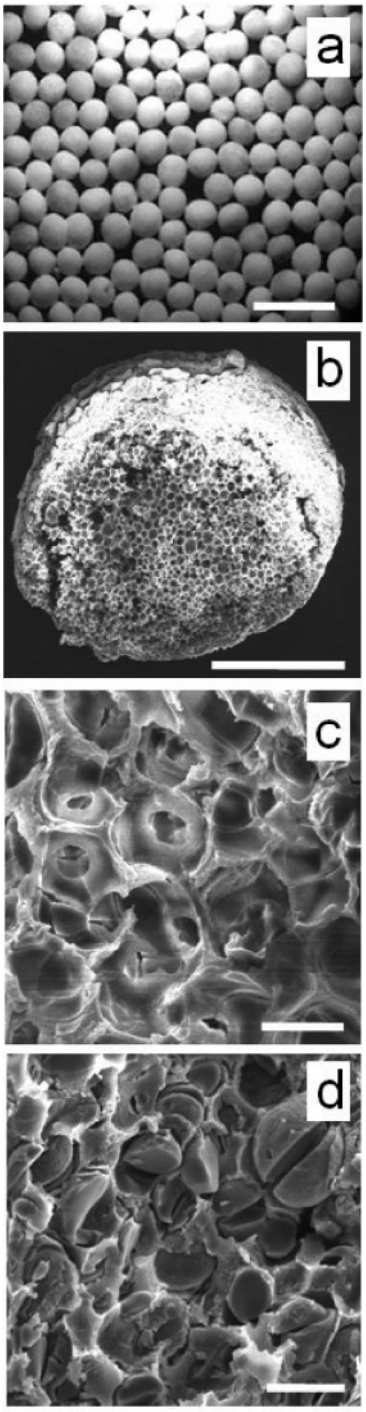

Figure 5. Bead morphology and pore structure of alumina beads: (a) optical image of alumina beads AlO-2 (scale bar = 5 mm). (b) Electron micrograph of cross-sectioned alumina bead AlO-2 showing internal structure (scale bar = 500 μm). (c) Electron micrograph of the internal structure of alumina bead AlO-2 (scale bar = 25 μm). (d) Electron micrograph of the internal structure of alumina beads that were made with less intensive washing. Most of the emulsion-templated cells are filled with entrapped alumina microparticles (scale bar = 25 μm).

(38) Deng, W.; Toepke, M. W.; Shanks, B. H. *Adv. Funct. Mater.* **2003**, *13*, 61−65.

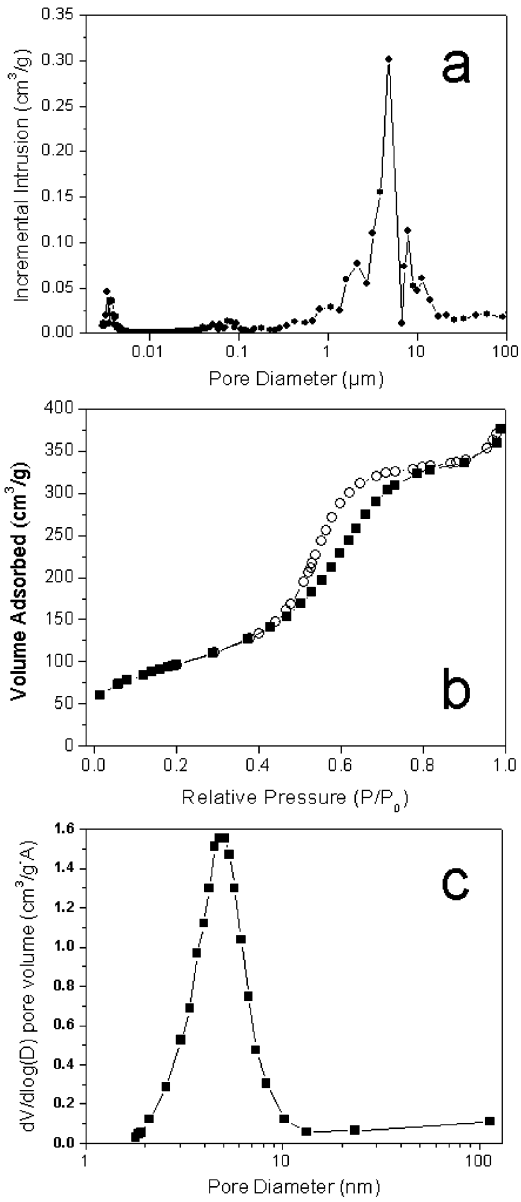

Figure 6. Pore size characterization of alumina beads: (a) plot of pore size distribution of AlO-2, calculated from mercury intrusion porosimetry data. (b) Adsorption (closed circles) and desorption (open circles) isotherms of alumina beads AlO-2. (c) Pore size distribution of alumina beads AlO-2 as calculated from N_2 sorption data using the BJH equation.

distribution of sample AlO-2 is shown in Figure 6c. The mesopores are in the range 2.0−10.0 nm, and the peak centers at around 4.0 nm. This is consistent with the results obtained by mercury intrusion porosimetry, which can only measure pores >7 nm diameter, hence the truncation of this peak in Figure 6a.

PEG−PPG−PEG was used as an auxiliary template to prepare AlO-2. However, the N_2 isotherm for AlO-2 was found to be very similar to that obtained for sample AlO-1 that was prepared without PEG−PPG−PEG.[32] The data suggest that samples AlO-1 and AlO-2 both contain mesopores of around 4 nm in diameter. It is possible therefore that the PEG−PPG−PEG template is not responsible for the formation of the narrowly distributed mesopores, although this auxiliary template did result in the formation of alumina beads with higher surface areas and larger pore volumes (Table 2).

Previously, silica and alumina mesostructures were prepared using the hydrolysis of the corresponding alkoxides in the presence of poly(ethylene oxide) (PEO) surfactants as structure-directing agents.[39] Amorphous silica−alumina materials with mesoporous distribution were also synthesized without using polymer templates.[28] The suggested mechanism was that these mesopores were formed from the rearrangement of primary particles. Alumina materials made from Al(O-*s*-Bu)$_3$-2,4-pentanedione-2-propanol-nitric acid system exhibited uniform mesopores of 2.9−7.4 nm at calcination temperatures of 400−1000 °C, while micropores were formed at lower calcination temperatures.[40] In our study, alumina beads with and without PEG−PPG−PEG as a template both exhibited narrowly distributed mesopores, which may arise from either rearrangement of primary particles or from the PAM scaffold.

The mesopores in the alumina beads (sample AlO-1) could also be observed by TEM (Figure 7a,b). These images suggest that the mesopores have a relatively narrow size distribution but are not well-ordered.

Al MAS NMR spectra of alumina beads (Figure 7c) were similar to those reported previously for mesoporous and mesostructured aluminas[41] and indicate the amorphous character of the inorganic component in both the composite and calcined materials. The broad peak at ca. 60 ppm is due to aluminum atoms in tetrahedral $[AlO_4]^-$ environments, and the resonance at ca. 5 ppm is from octahedrally coordinated aluminum.[28] The resonance at ca. 35 ppm can be ascribed to the aluminum with 5-fold coordination. The population of unsaturated 5-fold coordinate as well as tetrahedral Al sites increases after calcination. Such a structural rearrangement upon calcination might be of use for the application of the porous alumina beads in catalysis since the presence of the Al(5) sites has been speculated to be a source of the Lewis acidity in aluminas.[41b]

Titania Beads. Our two-step method was also successful for making hierarchically porous titania beads. This would have been impossible using our original one-step procedure[26] due to the much higher reactivity of the precursors toward water. Initially, neat Ti(O^{i}Pr)$_4$ precursor was used as the liquid to soak into the porous PAM beads. After soaking overnight, the polymer beads were filtered and washed with 2-propanol immediately. The titania beads obtained in this way showed porous internal HIPE structures, but there was a dense titania film blocking the porous surface. The titania film was composed of fine particles (1−5 μm), which could be observed by SEM.[32] This dense film resulted from the high reactivity of Ti(O^{i}Pr)$_4$ to moisture in the air that caused a rapid sol−gel process to occur before or during the washing procedure.

As a result, a Ti(O^{i}Pr)$_4$ solution in 2-propanol with or without an auxiliary template (PEG−PPG−PEG) was used to prepare TiO-2 and TiO-1 titania beads, respectively. For sample TiO-1, a HIPE internal structure was

(39) Bagshaw, S. A.; Prouzet, E.; Pinnavaia, T. J. *Science* **1995**, *269*, 1242−1244.
(40) Ji, L.; Lin, J.; Tan, K. L.; Zeng, H. C. *Chem. Mater.* **2000**, *12*, 931−939.
(41) (a) Vaudry, F.; Khodabandeh, S.; Davis, M. E. *Chem. Mater.* **1996**, *8*, 1451−1464. (b) Deng, W.; Bodart, P.; Pruski, M.; Shanks, B. H. *Micropor. Mesopor. Mater.* **2002**, *52*, 169−177.

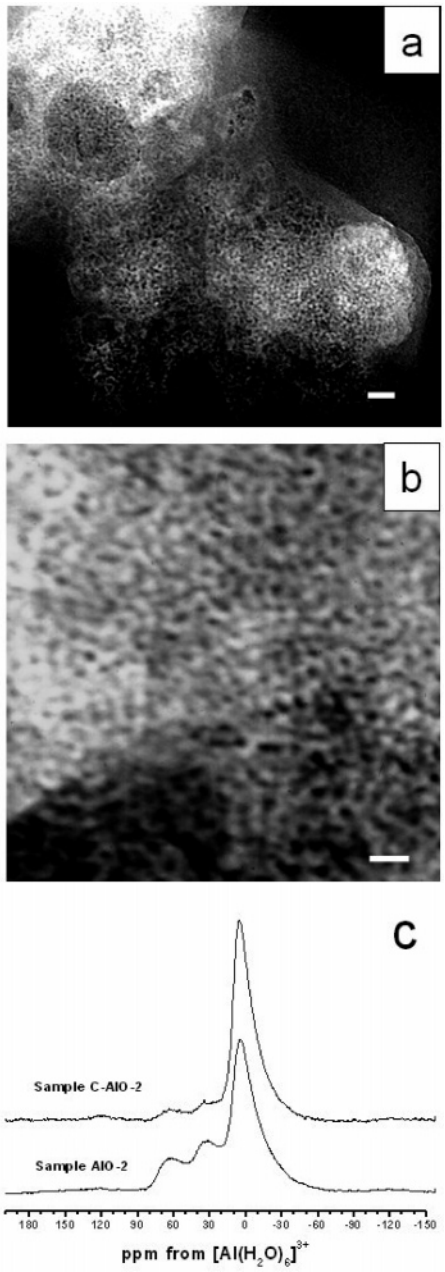

Figure 7. TEM images of alumina beads AlO-1: (a) scale bar = 20 nm. (b) Scale bar = 10 nm. (c) ^{27}Al MAS NMR spectra for samples AlO-2 and C-AlO-2.

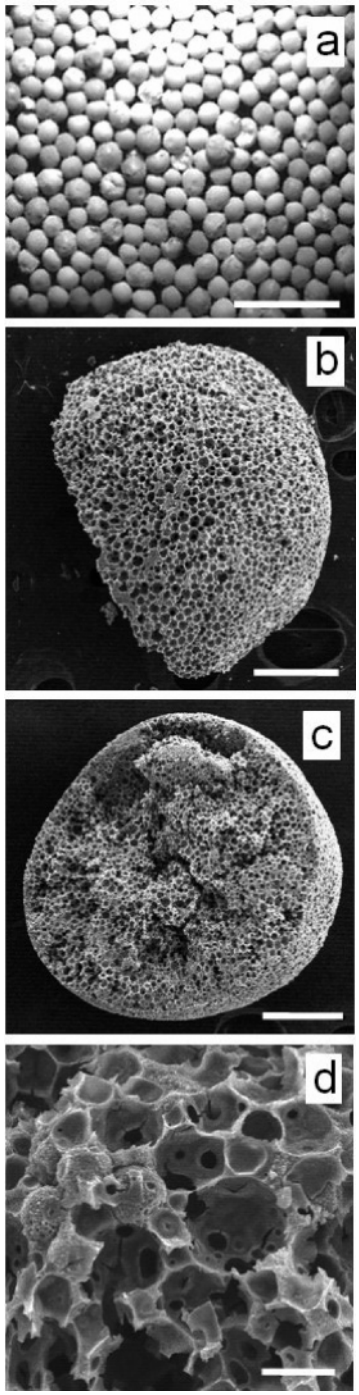

Figure 8. Bead morphology and pore structure of titania beads, TiO-2: (a) optical image (scale bar = 5 mm). (b) Electron micrograph of the bead surface (scale bar = 250 μm). (c) Electron micrograph of cross-sectioned bead showing the internal structure (scale bar = 250 μm). (d) Electron micrograph of the internal structure at higher magnification (scale bar = 25 μm).

replicated, and the surface was porous though some pores were still blocked.[32] When preparing TiO-2, the precursor solution was diluted three times with 2-propanol before filtering in air to reduce the viscosity of the solution. Figure 8a,b shows an optical image of the beads and the bead surface at a low SEM magnification, respectively, for sample TiO-2. It can be seen from Figure 8b that the bead surface is very porous and similar to the original PAM beads. The porous internal structure can be observed from Figure 8c, and SEM imaging at a higher magnification confirms that the macropores are interconnected (Figure 8d).

The pore size distribution measured by mercury intrusion porosimetry was bimodal, with peaks seen at 5 and 0.08 μm for TiO-1 and at 10 and 0.1 μm for TiO-2. For sample TiO-2, there was a very small peak at the high-pressure end of pore size distribution plot, which was also reflected in the cumulative intrusion curve.[32] As in the case of the alumina samples, this suggests the presence of mesopores in the sample that are slightly too small to be fully characterized by mercury intrusion porosimetry (<7 nm). The mesoporosity of sample TiO-2 is confirmed by the N_2 adsorption−desorption isotherms, which show a distinct hysteresis in the middle P/P_0 range (Figure 9a) and well-defined maximum at ~4.5 nm in the BJH plot (Figure 9b). For sample TiO-1, the adsorption curve rises slowly

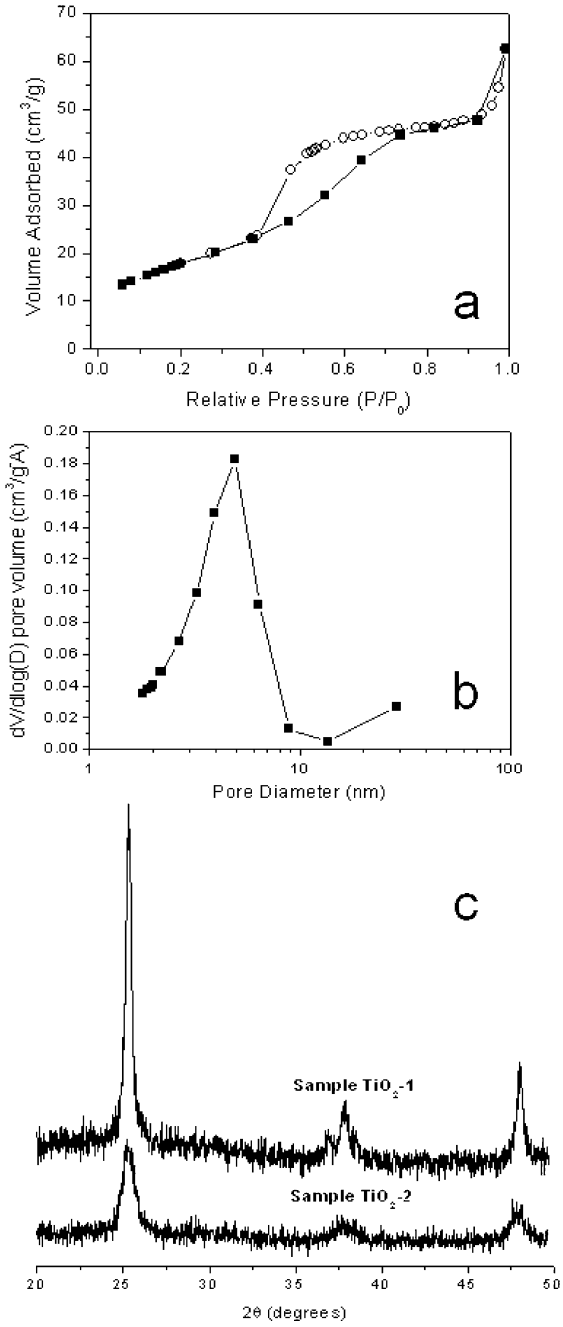

Figure 9. (a) Adsorption (closed circles) and desorption (open circles) isotherms for titania beads, TiO-2. (b) Pore size distribution calculated from N_2 sorption data using the BJH equation. (c) XRD patterns for titania beads TiO-1 (upper) and TiO-2 (lower).

in the middle relative pressure range ($P/P_0 = 0.4-0.7$), and the hysteresis is relatively small.[32] These data suggest that the presence of the block polymer resulted in higher surface areas and higher mesopore volumes, although as in the case of the alumina samples it is clear that some mesoporosity can be obtained without using the block copolymer template.

In previous studies, mesostructured titania was obtained by employing self-assembled structures of nonionic alkyl PEO surfactants as templates without any solvent.[42] The mesostructure was characterized by a distinct XRD pattern in the low angle region at $2\theta = 2°$.[42] Similarly, $TiCl_4$ and Pluronic F-127 were used to fabricate mesoporous thin films,[43] and wide-angle XRD in parallel mode clearly showed the formation of anatase by heating at 400 °C. In our study, the titania composite beads were calcined at 520 °C, and it was found that the materials were composed of the anatase phase, as confirmed by the XRD pattern shown in Figure 9c. From an approximate calculation using the Scherrer equation,[44] the crystallite size for sample TiO-1 was 19.6 nm and for sample TiO-2, 9.4 nm. There was no distinct XRD peak observed at low angle, which suggested that there were no ordered mesopores, although narrowly distributed mesopores are suggested by N_2 sorption analysis. By contrast, the uncalcined samples (C-TiO-1 and C-TiO-2) were composed of amorphous titania.

Zirconia Beads. Zirconia is known to play an important role as an industrial catalyst and as a catalyst support because of its moderate acidity and good ion-exchange properties. Much effort has been made to prepare ordered porous zirconia with a high surface area. To form a catalyst that has shape selectivity for large molecules in the same way that zeolites do for smaller molecules, narrow mesopore distributions are required.[43] For example, mesoporous sulfated zirconia was prepared with a maximum surface area of about 110 m^2/g by calcination at 650 °C.[29]

We prepared zirconia-PAM composite beads using a PEG−PPG−PEG auxiliary template followed by calcination at 520 °C. The resulting calcined zirconia beads had a surface area of 104 m^2/g with mesopores of approximately 2.5 nm in diameter, as calculated using the BJH method.[32] The isothermal plot showed a small hysteresis that supports the presence of mesopores. The mesopore diameter was smaller than observed for comparable alumina and titania beads. The zirconia beads prepared without using block copolymer template also showed mesopores[32] but exhibited lower surface areas and pore volumes, as observed for both alumina and titania (Table 2).

Large, emulsion-templated macropores were observed in addition to the mesopores in the uniform zirconia beads (10 and 0.08 μm for sample ZrO-1, 10 and 0.04 μm for sample ZrO-2).[32] Figure 10a shows an optical image of sample ZrO-2 with an average bead size of 1.11 mm. Figure 10b,c shows SEM images of this sample. The bead surface is partially macroporous with some pores covered by a denser zirconia film, but the internal structure is very macroporous, and the pores are highly interconnected (Figure 10c).

General Discussion. The objective of this work was to develop a generic method for preparing large, hierarchically porous inorganic beads. Emulsion-templated cross-linked PAM beads were used as templates to prepare inorganic composite beads, followed by calcination of the organic phase. It is quite surprising the emulsion-templated macropore structure is replicated in almost all cases, considering the low bulk-densities of the composite beads and the large mass loss that occurs during calcination (typically >50 wt. %). Before calcination, the precursors undergo sol−gel condensa-

(42) Dag, Ö.; Soten, I.; Çelik, Ö.; Polarz, S.; Coombs, N.; Ozin, G. A. *Adv. Funct. Mater.* **2003**, *13*, 30−36.

(43) Crepaldi, E. L.; Soler-Illia, G. J.; Grosso, D.; Sanchez, C. *New J. Chem.* **2003**, *27*, 9−13.

(44) Scherrer, P. *Gott. Nachr.* **1918**, *2*, 98−100

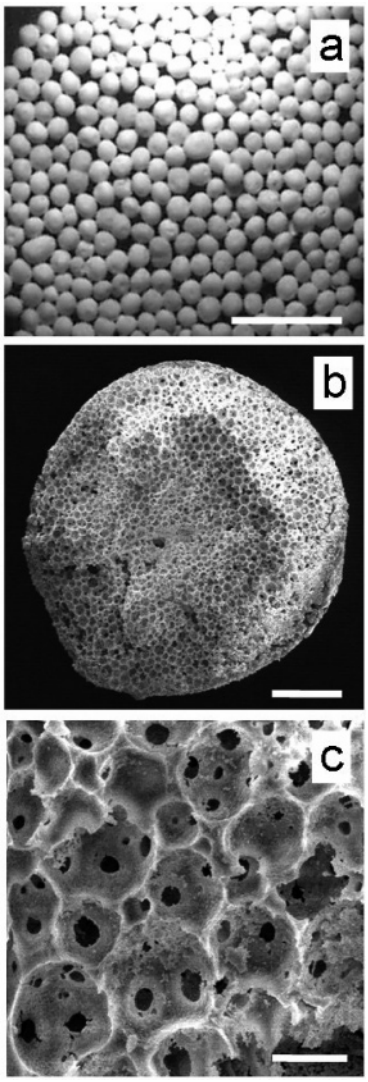

Figure 10. Bead morphology and pore structure of zirconia beads, ZrO-2: (a) optical image (scale bar = 5 mm). (b) Electron micrograph of cross-sectioned bead showing internal structure (scale bar = 250 μm). (c) Electron micrograph of internal structure at higher magnification (scale bar = 25 μm).

tion in air to form an inorganic network, which appears to be denser on the surface of the PAM material. The internal cell size was typically in the range 20−40 μm, and the emulsion-templated cells were highly interconnected. The windows connecting the cells, which were characterized by mercury porosimetry, were typically about 10 μm in diameter. The mesopores (if any) were found to be interconnected and open to larger macropores. This interconnectivity of pores is very important in potential reaction systems, both for large molecules and for small molecules.

It was expected that micropores would be obtained from the sol−gel chemistry and that ordered mesopores could be introduced by using a block copolymer auxiliary template, PEG−PPG−PEG. However, the results show that narrowly distributed mesopores are observed for all of the transition metal oxide beads, irrespective of whether PEG−PPG−PEG is used, although the auxiliary template does appear to increase the level of mesoporosity in most cases. Mesopore formation in the absence of PEG−PPG−PEG may arise from templating of the solvent-swollen cross-linked PAM matrix that is removed upon calcination or could result from the rearrangement of primary particles, as suggested for other template-free systems.[28] It is also possible that surfactant (Triton X-405) entrained in the PAM scaffold from the initial emulsion-templating process[25] plays an important role in the formation of mesopores.[39,43] For example, mesoporous silicates were prepared previously using Triton XN surfactants (Triton X45, Triton X114, and Triton X100) in the presence of concentrated mineral acids.[45] An important difference in our studies is that the Triton X-405 surfactant may be partially entrapped in the PAM matrix and thus less available for self-assembly and templating. Although the procedure for these preparing inorganic beads is relatively simple, it is clear that complicated, multiphase chemistry is involved in the evolution of these structures and that further studies regarding the detailed mechanism will be required.

Conclusions. This paper introduces a simple and potentially generic method to prepare large, uniform, inorganic beads (diameters 1.0−1.5 mm) with hierarchical porosity. The method is versatile for synthesizing silica beads and transition metal oxide beads (Al_2O_3, TiO_2, ZrO_2) and may be easily extended to prepare other organic−inorganic hybrid beads. Unlike our initial one-step method,[26] this new method does not require time-consuming reoptimization of emulsion stability for each new precursor that is used. Moreover, the new method permits the synthesis of materials from highly water-sensitive precursors such as $Ti(O^iPr)_4$, which could not possibly be used in a concentrated O/W emulsions.

The beaded morphology and the large macropores in the beads (about 10 μm) result from replication of the porous PAM scaffold. In some samples, additional narrowly distributed mesopores could be characterized by N_2 sorption. These pores may allow applications such as catalysis and molecular separation. Organic−inorganic composite beads were prepared before calcination, and these materials (or analogues) may themselves be very useful for certain applications.

The large beaded format of these materials allows for very simple handling and separation. We suggest that the highly interconnected emulsion-templated macropores will be particularly useful for applications that require large pore volumes or for use as supports in conjunction with macromolecules or viscous solutions where mass transport is limited in purely micro/mesoporous structures.

Acknowledgment. We gratefully acknowledge financial support from EPSRC (Research Grants GR/N39999 and GR/R15597). We also thank the Royal Society for provision of a Royal Society University Research Fellowship (to A.I.C). We thank the EPSRC for support of the North-West Molecular Materials Centre.

Supporting Information Available: Optical images, SEM images, BET data, and mercury intrusion porosimetry data. This material is available free of charge via the Internet at http://pubs.acs.org.

CM0492944

(45) Khimyak, Y. Z.; Klinowski, J. *J. Mater. Chem.* **2000**, *10*, 1847−1855.